Sand Drying Mechanism with Ambient Airflow

Ryuhei Hoshika, Ryo Horiguchi

Nikko Co., Ltd., Development Division, Development Section 4

Abstract

Japan has declared its commitment to carbon neutrality, aiming to reduce greenhouse gas emissions by 46% compared to 2013 levels by 2030 and to achieve net-zero emissions by 2050. Naturally, efforts to promote decarbonization are also advancing in the asphalt plant (hereinafter referred to as "AP") industry. As part of such efforts, our company has been working to reduce CO_2 emissions derived from fossil fuels by lowering the moisture content in sand before it enters the asphalt mixture production process by means of agitation and airflow into a kiln that operates at ambient temperature. This paper theoretically and experimentally investigates the mechanism by which moisture in sand evaporates when intake air comes into contact with the sand that falls in veil-like sheets from vanes that each have a J-shaped cross-section and are attached inside the rotating kiln at ambient temperature. Based on this investigation, we have developed a method to accurately estimate the amount of moisture evaporated from the sand.

1. Introduction

The amount of CO_2 emitted annually during the production of asphalt mixtures is approximately 1.5 million tons. Of this total, 79% originates from fossil fuels, 19% from electricity use, and 2% from other sources. Focusing on the CO_2 emissions from fossil fuels, which are the primary cause of these emissions, the energy used to heat and dry aggregates such as gravel and sand is distributed as follows: 37% for heating the aggregates, 42% for removing moisture, 15% for heating exhaust gases, 5% for heat loss, and 1% for heating water vapor[1]). This means that nearly half of the energy derived from burning fossil fuels is consumed in the removal of moisture from aggregates. From the perspective of the primary purpose, this energy consumption is a byproduct of aggregate heating and is considered reducible. Against this background, while the shift from fossil fuels to non-fossil energy sources is important, we believe that improving the energy efficiency of the aggregate drying process can significantly contribute to decarbonization in AP operations.

Based on the background described above, to reduce CO_2 emissions derived from fossil fuels, it is important to lower the moisture content of aggregates before they enter the asphalt mixture production process. To date, various countermeasures have been implemented, such as rainwater protection in stockyards and preferential use of the upper layers of stored aggregates—which tend to have relatively low moisture content—when feeding aggregates into storage hoppers. However, in cases where corrugated silos are used, or when further moisture reduction is required, we need to consider a more effective drying method that utilizes mechanical equipment. Therefore, we focused on a drying method using kilns, which is already available as equipment in AP facilities, that is expected to deliver a certain level of effectiveness.

Normally, heat exchange is carried out by bringing aggregates falling in veil-like sheets into contact with hot air generated by burner combustion, along with the rotation of a kiln as shown in **Figure 1**. In this paper, we focus on sand, which generally has a higher moisture content among aggregates, and use ambient airflow blown into the kiln (hereinafter referred to as "ambient airflow") as the heat exchange medium. In this case, the convective heat transfer between the surface of the sand and the air, as well as the total surface area of the dispersed sand that comes into contact with the ambient airflow retained in the kiln, are key factors influencing the amount of moisture to be evaporated from the sand. In this study, we determined the constant-rate drying rate and drying surface area of sand within the target kiln at ambient temperature, and constructed a simulation model to estimate the amount of moisture evaporated from the sand. Furthermore, we compared the simulation values with the results obtained from actual equipment testing so as to examine the accuracy of the model.

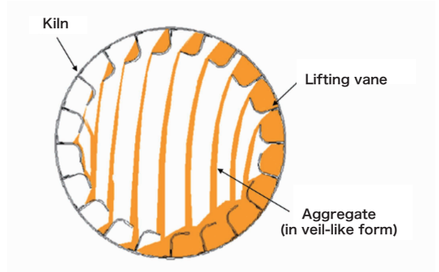

Figure 1: Distribution Pattern of Aggregate Inside the Kiln

2. Sand Drying Mechanism Using Ambient Airflow

Kilns are categorized into two types: the counterflow type, in which the airflow and sand move in opposite directions as shown in **Figure 2**, and the parallel flow type, in which both move in the same direction. Theoretically, the counterflow type has better thermal efficiency than the parallel flow type. Therefore, we have adopted the counterflow type in this paper. Accordingly, sand fed into the kiln moves forward while repeatedly rising and falling along with the kiln's rotation and comes into contact with the airflow. The kiln is inclined downward in the direction of sand movement.

Figure 3 shows the conditions of hot air and aggregates inside a counterflow-type kiln. Here, the hot air temperature is denoted as T, the aggregate temperature as Tm, the aggregate moisture content as w, and the absolute humidity of the hot air as H. In general, aggregates fed into a kiln undergo heat exchange with the hot air and proceed through a pre-heating period, constant-rate drying period, and falling-rate drying period so as to be dried. In other words, moisture evaporation from the aggregates begins at the end of the pre-heating period, when the aggregate temperature has risen from Tm_1 to Tm_2.

In contrast, **Figure 4** shows the conditions of airflow and sand when the sand is dried using ambient airflow. As in **Figure 3**, the ambient air temperature is denoted as T, sand temperature as Tm, sand moisture content as w, and absolute humidity of the ambient air as H. In this case, since the temperature difference between the sand fed into a kiln and the ambient air is small, the amount of heat transferred is also limited. Accordingly, the constant-rate drying period is expected to continue until the sand is discharged from the kiln. Furthermore, we predicted that the sand temperature would decrease from the inlet temperature Tm_1 to the wet-bulb temperature Tm_2 due to the evaporation of surface moisture, which absorbs latent heat. This period, in contrast to the pre-heating period in **Figure 3**, is defined as the pre-cooling period. The following section describes the constant-rate drying period after the end of the pre-cooling period.

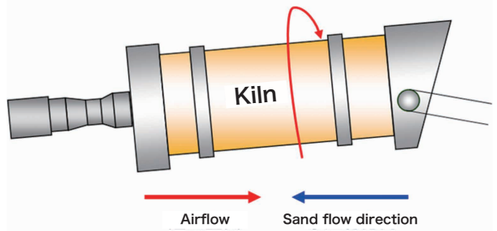

Figure 2: Image of the Kiln

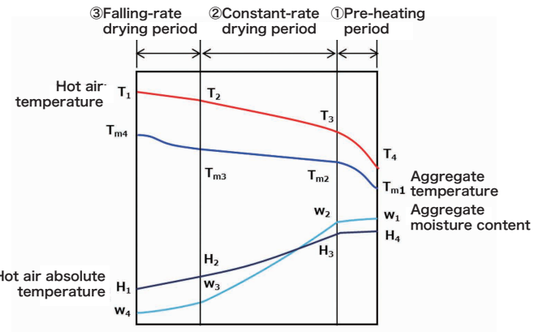

Figure 3: Internal State of the Kiln with Hot Air[2)]

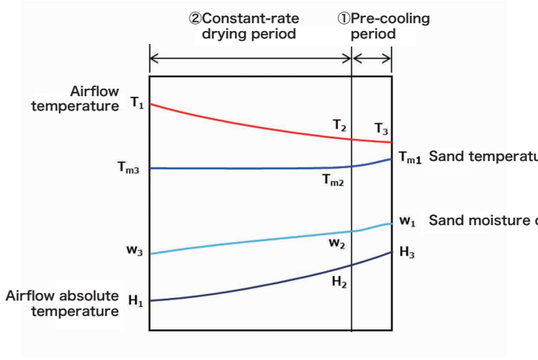

Figure 4: Internal State of the Kiln with Ambient Airflow

2.1 Constant-Rate Drying Period

2.1.1 Heat Exchange During the Constant-Rate Drying Period

During the pre-cooling period, the surface temperature of the sand decreases to the wet-bulb temperature, eventually reaching equilibrium. At this point, the amount of heat transferred to the sand via convective heat transfer from the ambient airflow is equal to the amount of heat consumed by the evaporation of moisture on the sand surface. This relationship can be expressed as: [Heat

transferred to the sand surface by convective heat transfer from ambient airflow] = [Heat consumed by evaporation of moisture on the sand surface]. This balance is represented by **Equation 1**[3]. The method for calculating representative physical property values used in the above equation will be described in the next section.

$$a \times h_c \times (T_2 - T_w) = a \times k_H \times (H_w - H_2) \times (\Delta h_v)_w \cdots [\text{Equation 1}]$$

where

a:Surface area of the sand in contact with ambient airflow (m^2)
hc:Convective heat transfer coefficient ($W/(m^2 \cdot K)$)
T_2:Temperature of the airflow at the end of the pre-cooling period (K)
Tw:Wet-bulb temperature of the sand (K)
k_H:Mass transfer coefficient (kg-water/($m^2 \cdot s \cdot \Delta H$))
Hw:Saturated absolute humidity at temperature Tw (kg/kg)
H_2:Absolute humidity at temperature T_2 (kg/kg)
$(\Delta hv)w$:Latent heat of vaporization at temperature Tw (J/kg)

2.1.2 Constant-Rate Drying Rate

In the equilibrium state described in the previous section, the amount of heat supplied remains constant. Accordingly, the moisture in the sand also evaporates at a constant rate. This is defined as the constant-rate drying rate, Jc, which can be expressed as **Equation 2** by rearranging **Equation 1**[4].

$$J_c = \frac{h_c \times (T_2 - T_w)}{(\Delta h_v)_w} \cdots [\text{Equation 2}]$$

where

Jc: Constant-rate drying rate ($kg/(s \cdot m^2)$)

2.2 Physical Property Values

This section describes the representative physical property values used in the calculation formula for the constant-rate drying period discussed in the previous section, along with the methods for calculating them.

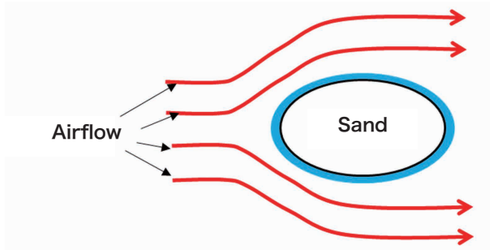

Figure 5: Contact Image

(1) Convective Heat Transfer Coefficient

Heat exchange at the surface of the sand occurs through forced convection as the sand comes into contact with ambient airflow passing through the kiln. Here, the sand falling in veil-like sheets from the lifting blades is assumed to be in a dispersed state, coming into contact with the flowing air: this can be modeled as air with a certain velocity contacting a single spherical sand particle as shown in **Figure 5**. Therefore, the convective heat transfer coefficient varies depending on the air velocity inside the kiln and the surface geometry of the sand particles.

In this case, the convective heat transfer coefficient is determined from the Nusselt number using **Equation 3**. Note that the Nusselt number itself is calculated using **Equation 4**, as given below[5].

$$h_c = \frac{(N_u \times \lambda)}{D} \cdots [\text{Equation 3}]$$

where

Nu:Nusselt number (m/m)
λ:Thermal conductivity of air ($W/(m \cdot K)$)
D:Diameter of a sand particle (m)

$$N_u = (2.7 + 0.12 \times Re^{0.66}) \times Pr^{0.5} \times \left(\frac{\mu}{\mu_s}\right)^{\frac{1}{4}} \cdots [\text{Equation 4}]$$

where

Re:Reynolds number (m/m)
Pr:Prandtl number (m/m)
μ:Viscosity coefficient of air (Pa·s)
μ_S:Viscosity coefficient of sand (Pa·s)
Note:The values of λ, μ, and μ_S are considered temperature-dependent with respect to air[6].

(2) Mass Transfer Coefficient

According to Lewis' relation, **Equation 5** is used[7].

$$k_H = \frac{h_c}{C_H} \quad : \quad C_H = C_{pg} + C_{pv} \times H \cdots [\text{Equation 5}]$$

where

C_H:Specific heat capacity of wet air (kJ/kg·K)
Cpg:Specific heat at constant pressure for air (kJ/kg·K)
Cpv:Specific heat at constant pressure for vapor (kJ/kg·K)
H:Absolute humidity (kg/kg)

(3) Latent Heat of Evaporation

The latent heat of evaporation $(\Delta hv)w$ is calculated by substituting the wet-bulb temperature Tw of the sand at the end of the pre-cooling period into **Equation 6**, which expresses the relationship between the water temperature and the latent heat of evaporation[8].

$$[(\Delta h_v)_w] = -2450 \times T_w + 3170072 \cdots [\text{Equation 6}]$$

2.3 Falling Range and Surface Area of Sand Inside the Kiln

According to **Equation 1**, the amount of moisture evaporated from the sand increases in proportion to the total surface area of the sand that comes into contact with ambient-temperature airflow after it is fed into the kiln and until it is discharged therefrom. Therefore, the surface area is a key factor in calculating the amount of evaporation. Below is a description of the falling range of the sand and the surface area of the sand falling in a veil-like form.

2.3.1 Falling Range of Sand

Figure 6 shows the cross-sectional area of a sand pile and the falling portion of the sand. As the kiln rotates, a portion of the cross-sectional pile of sand on each lifting vane exceeds the dynamic angle of repose, causing the sand portion to slip and fall from the vane.

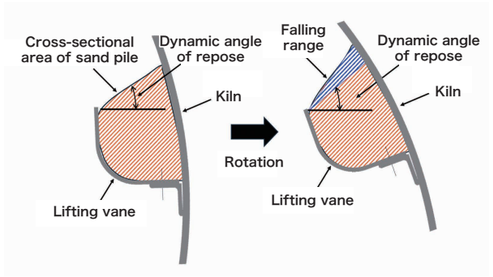

Figure 6: Sand Falling Range ①

Figure 7 illustrates the cross-section of sand piles inside a kiln. This cross-sectional area is calculated based on the kiln fill rate during ventilation. The fill rate depends on the amount of sand retained in the kiln and varies depending on whether the sand behavior is classified as Flight action or Kiln action. Accordingly, we need to determine which action we are handling. When the fill rate is smaller than the optimal fill rate for the lifting vanes, it is categorized as Flight action; when larger, it is Kiln action.[9]

Using this fill rate, the cross-sectional area of the sand pile As can be expressed by **Equation 7**, assuming that the cross-section of the sand piles occupies the 270° to 360° range of the kiln shown in **Figure 7**:

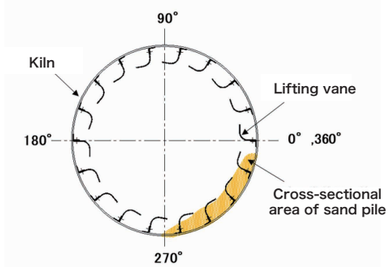

Figure 7: Cross Section of Sand Pile Inside the Kiln

$$A_s = \frac{(S \times X)}{\left(n \times \frac{1}{4}\right)} \cdots [\text{Equation 7}]$$

where

As: Cross-sectional area of the sand pile (m^2)
S: Cross-sectional area of the kiln (m^2)
X: Fill rate of the kiln during ventilation (%)
n: Number of lifting vanes (-)

As the kiln continues to rotate and the lifting vanes tilt further, the sand portion over the dynamic angle of repose, after beginning to fall, further slips down. This process repeats, causing the cross-section of the sand pile to decrease. Eventually, as shown in **Figure 8**, the angle between the dynamic angle of repose of the sand and the straight line extending from the vane tip to the curved section becomes equal. At this point, the falling of the sand from the lifting vane ends; this entire interval defines the falling range of the sand.

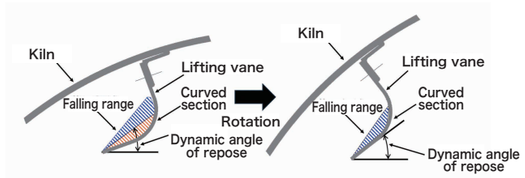

Figure 8: Sand Falling Range ②

2.3.2 Surface Area of Falling Sand

Figure 9 illustrates the range over which the sand falls. Here, the sand begins to fall at the lifting vanes and continues through an angular range of θ°. Within this range, n lifting vanes are arranged in total. If the one-sided surface area of the sand falling in a veil shape from a single vane is denoted as a_i, as shown in **Figure 10**, the total surface area Aagt of the veil-like falling sand from the lifting vane can be expressed by **Equation 8**:

$$A_{agt} = 2 \times \sum_1^n a_i \cdots [\text{Equation 8}]$$

where

Aagt: Total surface area of the falling sand (m^2)
a_i: One-sided surface area of the sand falling from a single lifting vane (m^2)

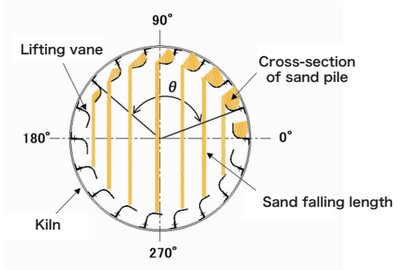

Figure 9: Sand Falling Range

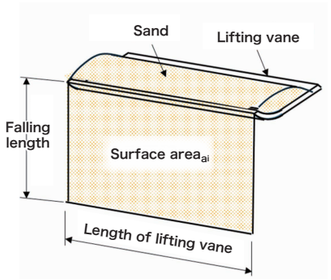

Figure 10: Sand Surface Area

3. Simulation Model

In this section, we estimate the amount of moisture evaporated from sand using the equations defined in Chapter 2. First, we calculate the convective heat transfer coefficient and the latent heat of evaporation based on the test conditions as described later. These values are then substituted into **Equation 2** to determine the constant-rate drying rate. This allows us to calculate the amount of moisture evaporated per unit time and per unit surface area.

Next, within the region where lifting vanes are installed, the falling range of sand is determined according to the number of vanes arranged. Using **Equation 8**, the drying surface area of the falling sand is calculated and then multiplied by the residence time. The product is further multiplied by the constant-rate drying rate, and the amount of moisture evaporated is estimated.

3.1 Simulation Conditions

The simulation was conducted under the same conditions as those used in the actual equipment testing described later. **Table 1** shows the test conditions.

Table 1 Test Conditions

Test Date	11/06/2024
Weather	Sunny
Ambient Temperature	25°C
Ambient Humidity	67%
Sand Temperature	20°C
Sand Particle Size	0.0006 m
Moisture Content Ratio	2.37%
Feed Rate	15 t/h
Test Duration	20 min
Airflow in Kiln	412 Nm³/min
Kiln Shell Temperature	23°C
Kiln Rotation Speed	6.7 rpm

Figure 11 shows an overview of the kiln used in this simulation. The kiln has a wall thickness of 16 mm, an outer diameter of ϕ2150 mm, and a length of 7500 mm, and is inclined at 4° in the direction of sand movement. **Figure 12** illustrates the arrangement of the lifting vanes. Here, the region targeted for calculating the sand drying surface area is limited to the lifting vanes that have a J-cup shape. These vanes are arranged at intervals of 40° (9 divisions), 20° (18 divisions), and 12.9° (28 divisions) from the sand inlet side, where the vane lengths are 910 mm, 920 mm, and 2330 mm, respectively.

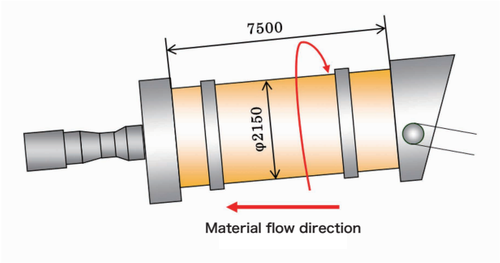

Figure 11: Overview of the Kiln

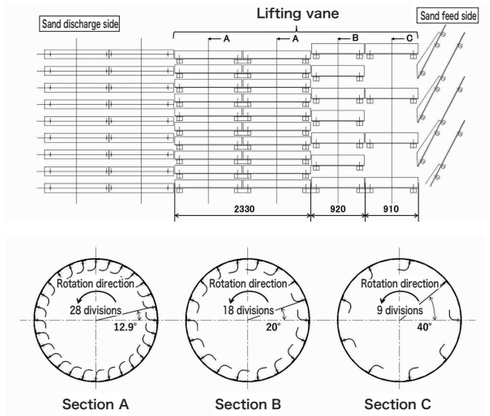

Figure 12: Lifting Vane Arrangement

3.2 Simulation Results

Table 2 shows the results calculated under the same conditions as the actual equipment testing.

Table 2 Calculation Results

Thermal Conductivity	79.5 W/m²K
Wet-Bulb Temperature	289.15 K
Latent Heat of Evaporation	2461655 J/kg
Constant-Rate Drying Speed	0.00029 kg (s·m²)
Drying Area	44.34 m²
Amount of Evaporation	0.0129 kg/s
Reduced Moisture Content Ratio	0.25%

The reduction in moisture content was calculated to be 0.25% based on the constant-rate drying rate and drying surface area of the sand predicted by the simulation model.

4. Actual Test Results and Simulation Evaluation

Under the test conditions shown in **Table 1**, sand was fed into the kiln at ambient temperature, and the temperature and moisture content of the sand discharged through the extraction mechanism at the kiln outlet were measured. The results are shown in **Table 3**.

Table 3 Test Results

Moisture Content Ratio		Reduced Moisture Content Ratio	Sand Temperature
Before feeding	After Drying		
2.37%	2.10%	0.27%	20°C

According to **Table 3**, the reduction in moisture content achieved using the ambient-temperature kiln was 0.27%. The difference from the value predicted by the simulation model was 0.02%. This error is 6.9% when expressed as a percentage. Based on the obtained value, the simulation model can be considered highly accurate. Furthermore, the temperature of the discharged sand remained at 20°C, the same as before it was fed into the kiln.

5. Discussion

The comparison between the results of actual equipment testing and the predicted values from the simulation model verified that the simulation model has a high degree of accuracy. This indicates that both the constant-rate drying rate and the drying surface area of sand, derived during the process of estimating the amount of moisture evaporation, are reasonable values. We believe that combining multiple theoretical equations to model the sand drying phenomenon in a kiln at ambient temperature contributed to the high reproducibility of the predictions. Additionally, the temperature of the sand discharged from the kiln outlet was 20°C, the same as its temperature before entering the kiln. This was 4°C higher than the predicted value of 16°C. This discrepancy is likely attributable to the time delay between the discharge of the sand from the kiln outlet and the temperature measurement, as well as potential measurement errors.

6. Future Work

To achieve decarbonization in AP operations, a rational approach is to improve energy efficiency in the aggregate drying process. In this paper, we examined the mechanism by which moisture contained in sand evaporates through exposure to ambient airflow inside the kiln. In addition, a simulation model was developed by combining defined equations to estimate the amount of moisture evaporation. Finally, by comparing the model results with actual testing results, the accuracy of the simulation model' s predictions was evaluated. As a result, the margin of error was found to be 6.9%, confirming that a highly accurate simulation model was successfully established. However, the reduction in moisture content was less than 0.3%, meaning that the amount of heat contributing to the drying performance was negligible. This result clarified that a greater amount of heat is essential to achieve the expected drying effect.

To enhance the sand drying performance, we are planning to investigate the use of residual heat stored in a kiln immediately after asphalt mixture production. The temperature of the kiln shell just after the operation exceeds 100°C, and this heat is potentially usable. However, with increased moisture evaporation from the sand, the absolute humidity inside the kiln will rise. This raises concerns about condensation in dust collection equipment. Therefore, we intend to proceed with these efforts while also ensuring the stability of plant operations.

References

1) Road Construction. (2021). Efforts Toward Decarbonization in Asphalt Plants (No. 788, pp. 50–51).
2) Tatemoto, Y., & Nakamura, M. (2013). Learning Drying Technology from the Basics: Fundamentals and Practice (2nd ed., p. 139). Maruzen Publishing.
3) Tatemoto, Y., & Nakamura, M. (2013). Learning Drying Technology from the Basics: Fundamentals and Practice (2nd ed., p. 32). Maruzen Publishing.
4) Tatemoto, Y., & Nakamura, M. (2013). Learning Drying Technology from the Basics: Fundamentals and Practice (2nd ed., p. 37). Maruzen Publishing.
5) Academic Press. (2020). Heat transfer: Principles and application (p. 214).

6) Microelectronics Heat Transfer Lab. (1984). Properties of Dry Air at One Atmosphere (p. 1).
7) Tatemoto, Y., & Nakamura, M. (2013). Learning Drying Technology from the Basics: Fundamentals and Practice (2nd ed., p. 33). Maruzen Publishing.
8) Kochi University, Laboratory of Environmental Chemistry. Website of Tanimizu. M. (Accessed on December 26, 2024). Saturated Vapor Pressure of Water.
9) Kiritaka, R. (1966). Drying equipment (pp. 142–144). Nikkan Kogyo Shimbun.

Authors

HOSHIKA, Ryuhei
Development Division, Development Section 4
(Joined Nikko Co., Ltd. in 2019)

HORIGUCHI, Ryo
Development Division, Development Section 4
(Joined Nikko Co., Ltd. in 2011)

MEMO